行政院國家科學委員會專題研究計畫成果報告

超音波非線性影像

Ultrasonic Non-Linear Imaging

計畫編號：NSC 88-2314-B-002-216-M08
執行期限：87 年 8 月 1 日至 88 年 7 月 31 日
主持人：李百祺　　台灣大學電機工程學系

一、中文摘要

由有限振幅失真所產生之第二諧波訊號以水聽筒測量並發現其聲場強度之分布與探頭大小及聚焦深度有直接的關係。仿體影像及電腦模擬亦顯示，動態發射聚焦可以在不顯著影響影像對比之情形下大幅提高第二諧波訊號之靈敏度。

關鍵詞：超音波、非線性影像、多重聚焦

Abstract

Generation of the second harmonic signal was studied for finite amplitude distortion based second harmonic imaging. Acoustic field amplitudes of a fixed focus transducer along the range axis were measured using a PVDF needle hydrophone. Results indicated that on-axis amplitudes strongly depended on the f-number at both the fundamental and the second harmonic frequencies. A two-focus transducer was also used. Gray scale imaging, hydrophone measurement and simulations were performed. Results of the study using the two-focus transducers can be generalized to imaging systems with full dynamic transmit focusing capabilities. It is expected that dynamic transmit focusing can improve the SNR of finite amplitude distortion based second harmonic imaging while improving the contrast resolution over fundamental imaging.

Keywords: Ultrasound, Nonlinear Imaging, Multiple Zone Focusing.

二、緣由與目的

The use of finite amplitude distortion based second harmonic imaging has been successful in clinical ultrasound [1-3]. Such an imaging method is also known as tissue harmonic imaging. Tissue harmonic imaging has become popular due to its ability to markedly improve image quality. In this project, effects of transmit focusing on the second harmonic signal generated through nonlinear propagation are investigated. Both hydrophone measurements and pulse-echo phantom imaging are performed. Characteristics of the second harmonic field amplitudes are compared to the fundamental field amplitudes for transducers with different focal depths. Extensive simulations are also performed to study the effectiveness of second harmonic generation using a two-focus array transducer. The potential degradation in contrast resolution is also addressed.

三、方法

Hydrophone measurements were done to study effects of transmit focusing on second harmonic generation. An arbitrary function generator was used to generate a Gaussian signal. The signal had a center frequency at 2 MHz and a 37% fractional bandwidth. Spectrum of the Gaussian signal is shown as the dashed line in Figure 1. Note that the bandwidth was chosen such that there was insignificant overlap between the fundamental bandwidth and the second harmonic bandwidth generated through

nonlinear propagation. The Gaussian signal was sent to a power amplifier to drive a 2.25 MHz focused transducer. The transducer had a diameter of 29 mm and was geometrically focused at 70 mm. Acoustic fields in water were measured by a PVDF needle hydrophone with a 30 dB pre-amplifier gain. Position of the hydrophone was controlled by a three-axis step motor system with a 5 «m step size. The amplified signal is then digitized by a 20 Msamples/sec analog-to-digital converter with 12-bit resolution. A Pentium-class personal computer was used to control the three-axis step motor system and to communicate with the VXI mainframe via the VEE software.

Using the RF signal acquired at each measurement point, both the spectrum and the amplitude of the signal can be obtained. At each depth, the acoustic field was measured over a 10 mm by 10 mm area. The spacing between two adjacent measurement points was 0.15 mm. Along the center axis of the transducer the field was measured from 2 mm to 100 mm with a 2 mm step size. The solid line in Figure 1 shows the measured spectrum at the focal point. Compared to the original Gaussian spectrum, nonlinear effects are apparent as the peak of the second harmonic component increases from virtually zero to about –27 dB relative to the peak of the fundamental signal.

Pulse-echo imaging was also performed. The setup is similar to the previous one except for the following differences. First, the transducer operated in pulse-echo mode. Hence, two diodes were connected backward to isolate the electronic noise from the power amplifier to the receiver. Second, the transducer had a center frequency of 3.5 MHz. Since it was operated in the pulse-echo mode, both the fundamental and the second harmonic signals must be within the transducer's passband. To meet this requirement, the transmitted waveform was a Gaussian pulse with a center frequency of 2.25 MHz and the fractional bandwidth was 42%. On receive, the second harmonic bandwidth was centered at 4.5 MHz. The image phantom was gelatin based containing glass beads as sound scatterers. The glass beads were with a diameter less than 106μm. There was a cylindrical, anechoic cyst parallel to the surface of the phantom. The secondary focus is made by adding silicon rubber to the center portion.

The simulation model is similar to the model used in [1,2]. The model accounts for pulse sources with arbitrary frequency response and approximates continuous beam formation by incremental field propagation. At each incremental step, linear propagation is calculated based on the angular spectrum method and the nonlinear propagation is simulated based on the finite amplitude propagation model. Propagation was assumed in water and no attenuation effect was included in the simulations. The nonlinear parameter was set to 3.5 approximating the nonlinear property of water.

In all simulations, a one-dimensional, 96 channel linear array was assumed. The array had a 0.25 mm pitch and the primary focus was 60 mm away from the transducer. The transmitted waveform had a Gaussian envelope with a 2 MHz center frequency and a 47% fractional bandwidth. The source plane peak amplitude of the Gaussian waveform was 20cm/sec

四、結果與討論

The normalized on-axis amplitudes are shown in Figures 2 and 3 as the solid lines. Figure 2 shows the fundamental signal amplitude (i.e., the amplitude at 2 MHz) and Figure 3 shows the second harmonic amplitude (i.e., the amplitude at 4 MHz). At each depth, the local spatial peak was used as the on-axis amplitude. Compared to the fundamental amplitude, the second harmonic amplitude increases rapidly prior to the focus and declines slowly after the focus. The peak position of the second harmonic profile is slightly deeper than the focal depth. Clearly, amplitude of the second harmonic signal generated through nonlinear propagation

cannot be simply approximated by the square of the amplitude of the fundamental signal.

The phantom images are shown in Figures 4 and 5. The top panel corresponds to the single focus transducer and the lower panel is for two-focus transducer, which was produced by adding a layer of silicon rubber at the center portion of the transducer. All images are displayed over a 30 dB dynamic range and no depth dependent gain was applied. The secondary focus effectively increased the near field amplitude and the amplitude declined rapidly after 60 mm. For optimal amplitude distribution, the choice of focal depths must be determined based on specific imaging requirements.

Simulation results of Arrays 1 (single focus), 2 (secondary focus at 20mm) and 3 (secondary focus at 30mm) are shown in Figures 6 and 7. The upper panel in Figure 6 shows the on-axis amplitudes at the fundamental frequency and the lower panel shows the second harmonic amplitudes. In both panels, the solid line represents Array 1, the dot-dashed line denotes Array 2 and the dashed line is for Array 3. Although the peak instantaneous pressure was the same for all cases, the secondary focus effectively increased the second harmonic generation as shown in the lower panel. Moreover, the second harmonic amplitude continued to increase throughout the entire range. Therefore, it is shown that both the near field harmonic signal and penetration were improved by adding the secondary focus.

Effects of the secondary focus on contrast resolution are shown in Figure 7. The idea was to use normalized integrated magnitude of the lateral radiation pattern to evaluate contrast resolution. The integration starts from the center of the ultrasound beam (i.e., the range axis) and ends at a pre-specified lateral position. Using such a representation, a profile rises rapidly to unity represents low sidelobes and hence better contrast resolution.

Normalized integrated magnitudes of Array 1, Array 2 and Array 3 are shown in Figure 7 as the solid line, the dashed line and the dot-dashed line, respectively. In addition, the dotted line shows the normalized integrated magnitude of the 4 MHz radiation pattern from linear propagation. In general, the secondary focus degraded beamforming quality and resulted in a slower curve. Compared to the dotted line, nevertheless, all the second harmonic radiation patterns had better contrast resolution. In other words, although the image quality was degraded by the addition of the secondary focus, the resulting contrast resolution of the second harmonic beam was still better than that of the linear beam at the same frequency. Thus, amplitudes of the second harmonic signal can be increased while maintaining the contrast resolution enhancement. The tradeoff between the increase in second harmonic amplitude and the slight decrease in image contrast is determined by specific imaging requirements.

五、計畫成果自評

Nonlinear propagation models were simulated and acoustic fields were measured using a hydrophone and pulse-echo imaging. Efficacy of dynamic transmit focusing on increasing second harmonic generation was clearly shown. The results have been submitted to Ultrasonic Imaging for consideration for publication.

六、參考文獻

[1] T. Christopher, “Finite amplitude distortion-based inhomogeneous pulse echo ultrasonic imaging”, *IEEE Trans. Ultrason., Ferroelect., Freq. Contr.*, Vol. 44, No. 1, pp. 125-139, 1997.

[2] P.-C. Li, “Pulse compression for finite amplitude distortion based harmonic imaging using coded waveforms”, *Ultrason. Imaging*, Vol. 21, No. 1, pp. 1-17, 1999.

[3] F. Tranquart, N. Grenier, V. Eder and L. Pourcelot, “Clinical use of ultrasound tissue harmonic imaging”, *Ultrasound Med. Biol. 25,* 889-894 (1999).

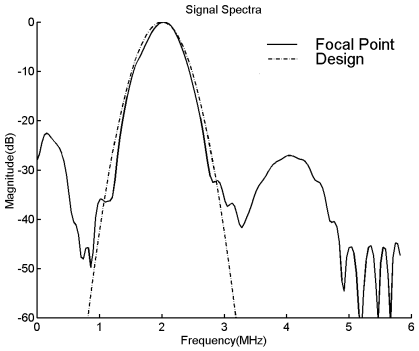

Fig. 1

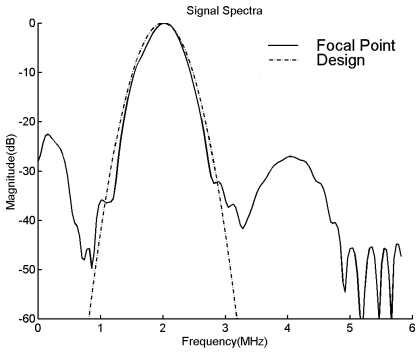

Fig. 2

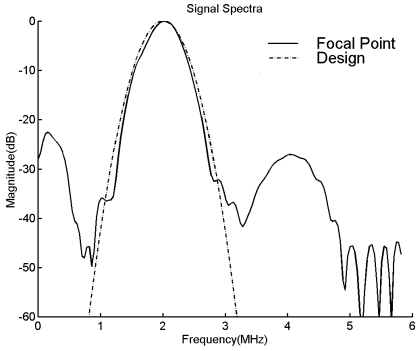

Fig. 3

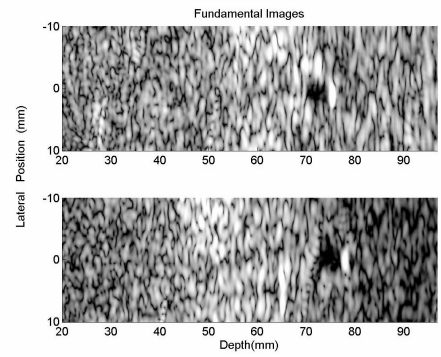

Fig. 4

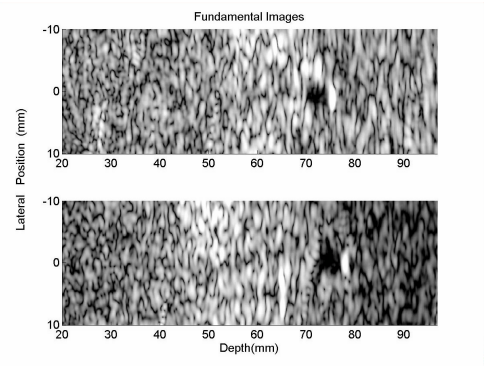

Fig. 5

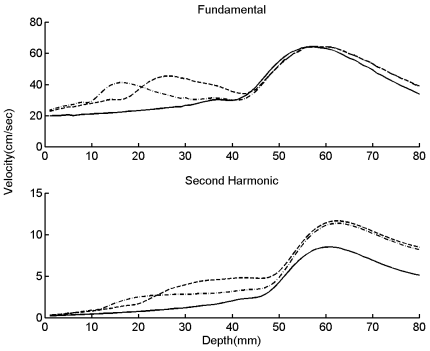

Fig. 6

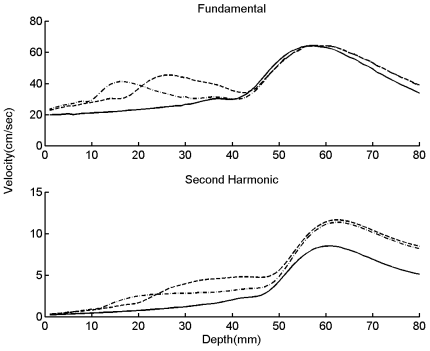

Fig. 7